CrossMark

Experimental investigation and thermodynamic modeling of the Al–Dy–Zr system

H. Bo[1,2] · L. B. Liu[2] · J. L. Hu[3] · Z. P. Jin[2]

Abstract The Al–Dy–Zr ternary system has been experimentally studied and thermodynamically assessed to contribute to the development of novel heat-resistant aluminum alloys. Using equilibrated alloys, the isothermal section of this ternary system at 873 K has been established by means of scanning electron microscopy/energy-dispersive X-ray spectroscopy (SEM/EDX) and X-ray diffraction (XRD). Experimental information on vertical sections was obtained by performing differential scanning calorimetry (DSC) analysis on selected annealed samples and that on liquidus projection was extracted from the as-cast samples by observing the primary crystallization phases. In addition, the first-principles method was employed to calculate the enthalpy of formation of metastable compounds involved in the sublattice model. Based on the experimental data and first-principles calculation results in this work, the Al–Dy–Zr system was optimized within the framework of the calculation of phase diagram (CALPHAD) method. Good agreement was found between the experimental data and the thermodynamic calculation results, which indicates that the thermodynamic description developed in this work is reliable.

✉ H. Bo
bohong@ysu.edu.cn

1 State Key Laboratory of Metastable Materials Science and Technology, and College of Materials Science and Engineering, Yanshan University, Qinhuangdao 066004, Hebei, People's Republic of China

2 School of Materials Science and Engineering, Central South University, Changsha 410083, Hunan, People's Republic of China

3 College of Mechanical and Electrical Engineering, Central South University, Changsha 410083, Hunan, People's Republic of China

Introduction

To increase the strength of aluminum alloys at elevated temperatures has always been a hot topic in the research filed of light metals, since this would increase the service temperature and expand the scope of their application. Studies show that microalloying is a feasible way to increase the mechanical properties to some extent [1–6]. As is widely accepted, scandium is the most effective alloying element in Al alloys since the Al_3Sc phase with an $L1_2$ structure that is coherent with the matrix will be uniformly precipitated after the addition. However, the application of Sc-containing aluminum alloys is limited to aerospace and sports equipment due to the high price of Sc itself. Therefore, it is of great importance to seek substitutes of Sc to lower the cost [7–11]. As stated by Knipling et al. [12], Zr is the optimum candidate for the following four reasons. First of all, the diffusion coefficient of Zr in Al is small. Secondly, the metastable $L1_2$–Al_3Zr phase could be formed with a lattice parameter mismatch between itself and the matrix of only 0.75 %. Thirdly, the small solubility of Zr in Al is conducive to the precipitation strengthening in the as-cast alloys. The last reason is the low cost of Zr. It should be noted that the $L1_2$–Al_3Zr phase could only be obtained through a special technology such as the rapid solidification. The addition of the rare-earth elements such as Dy, Ho, and Tb into the Al–Zr alloys could have a stable $L1_2$ phase formed, as reported in literatures [13–16], which may provide an opportunity of improving the strength of aluminum alloys at high temperatures with low-cost conventional casting. The present work centers on the thermodynamic study of the Al–Dy–Zr system, hoping that the establishment of a reliable thermodynamic description of this ternary system would provide guidance for the development of novel heat-resistant aluminum alloys.

🍎 Springer

Review of the Al–Dy–Zr ternary system

Several authors have investigated the isothermal section of the Al–Dy–Zr system at 773 K, including Tyvanchuk et al. [13], Yuan et al. [14], and Hu et al. [15]. In the isothermal section over 67–100 at.% Al as reported by Tyvanchuk et al. [13], there is a ternary compound of $Al_{30}Dy_7Zr_3$ with an $L1_2$ structure. Around it are four three-phase regions, namely $Al+Al_3Zr+Al_{30}Dy_7Zr_3$, $Al+Al_3Dy+Al_{30}Dy_7Zr_3$, $Al_3Zr+Al_{30}Dy_7Zr_3+Al_2Dy$, and $Al_3Dy+Al_{30}Dy_7Zr_3+Al_2Dy$. In the Al_2Dy phase, Zr could substitute Dy to a great extent with a large solubility of Zr up to about 20 at.%. By contrast, the solubility of Zr in the Al_3Dy phase is only about 1 at.% and that in the Al_3Zr and Al_2Zr phases is none. Recently, Yuan et al. [14] and Hu et al. [15] separately investigated the isothermal section over the entire composition range by SEM/EDX and XRD. In the Al-rich corner, the phase relations reported by Yuan et al. [14] are the same as those reported by Tyvanchuk et al. [13]. Similar results were obtained in the work of Hu et al. [15], where the two-phase field of $Al_3Zr + Al_2Dy$ is narrowed to be a line instead of a noticeable region in other work [13, 14]. Over 50–67 at.% Al, the phase relations determined by Hu et al. [15] and Yuan et al. [14] are generally consistent with each other. For the content of Al less than 50 at.%, only the three-phase fields of $AlDy + AlZr + Al_3Zr_4$, $Dy + Zr + AlZr_3$, and $Dy + AlZr_3 + AlZr_2$ exist in both of their work and nothing in common is shared for the phase relations in the rest of the region, which is encompassed by Dy–$AlDy$–Al_3Zr_4–$AlZr_2$–Dy. In addition, many differences could be noticed in the measured maximum solubility of a third component in Al–Dy and Al–Zr binary compounds comparing these two studies. According to Yuan et al. [14], the Al–Dy binary compounds all have homogeneity range and none of the Al–Zr compounds does. However, Hu et al. [15] reported a homogeneity range in three Al–Dy phases, i.e., Al_3Dy, Al_2Dy, and $AlDy$, four Al–Zr compounds, i.e., Al_3Zr, Al_2Zr, Al_3Zr_2, and $AlZr_2$, and Zr as well. For the three compounds Al_3Dy, Al_2Dy, and $AlDy$ that were found to have a homogeneity range in both of their work, the maximum solubility of Zr was measured to be 2.5, 22.5 and 2.4 at.%, respectively, by Yuan et al. [14], and 2, 26 and 3 at.% by Hu et al. [15].

The Al-rich corner of this ternary system has been thermodynamically optimized in our previous work [17], where the Al–Dy binary was re-assessed and the Dy–Zr binary was assessed for the first time. This assessment would mainly focus on the region beyond the Al-rich corner.

Experimental procedure

Eighteen individual alloys were prepared by arc-melting under argon atmosphere, with 99.99 wt.% purity of Al, Dy, and Zr as starting materials. Among them, the samples 1–9# were designed to weigh 3.8 g, and 10–18# 4.3 g. The nominal compositions of the samples are listed in Table 1, where the actual compositions measured by SEM/EDX are given as well for comparison. The difference between the nominal and actual composition with regard to constituent elements is not more than 2.5 at.% for all the samples except 15# and 16#. On the whole, there is a greater change in the atomic percent of the element Al than that of Dy or Zr after melting.

Each of the produced samples was cut into two pieces. One of them was sealed in an evacuated and argon-refilled quartz tube and annealed at 873 K for 1440 h, followed by water quench. After that, it was divided into pieces again and examined by SEM/EDX, XRD, and DSC. The FEI Quanta-200 SEM/EDX was used to observe the microstructure of the annealed samples and determine the equilibrium phase constitution. First, a low magnification was set to measure the compositions of three selected areas and the average value was calculated to approximately represent the actual composition of a sample as given in Table 1. Then, the magnification was raised to observe the microstructure and measure the compositions of

Table 1 Nominal and actual compositions of individual alloys

Alloy no.	Nominal composition (at.)			Actual composition (at.)		
	Al	Dy	Zr	Al	Dy	Zr
1#	0.776	0.176	0.048	0.799	0.160	0.041
2#	0.800	0.100	0.100	0.825	0.093	0.082
3#	0.783	0.063	0.154	0.800	0.063	0.137
4#	0.735	0.212	0.053	0.756	0.195	0.049
5#	0.719	0.143	0.138	0.735	0.134	0.131
6#	0.693	0.221	0.086	0.715	0.210	0.075
7#	0.691	0.043	0.266	0.699	0.041	0.260
8#	0.638	0.124	0.238	0.650	0.118	0.232
9#	0.650	0.042	0.308	0.655	0.043	0.302
10#	0.604	0.249	0.147	0.621	0.243	0.136
11#	0.540	0.122	0.338	0.550	0.112	0.338
12#	0.452	0.439	0.109	0.473	0.423	0.104
13#	0.473	0.098	0.429	0.480	0.092	0.428
14#	0.376	0.467	0.157	0.401	0.453	0.146
15#	0.296	0.467	0.237	0.334	0.434	0.232
16#	0.324	0.128	0.548	0.350	0.100	0.550
17#	0.270	0.080	0.650	0.286	0.076	0.638
18#	0.153	0.110	0.737	0.163	0.106	0.731

constituent phases. The accelerating voltage for SEM is set to 20 kV and the size of the beam spot 5.0 or 6.0 Å. To support the conclusion on phase constitution drawn from the SEM results, the XRD experiments were performed on the D/Max2500DC instrument with a Cu K$_\alpha$ radiation. The scanning is from 10° to 90° at a step of 8° min^{-1}, with a voltage of 40 kV and a current of 250 mA. Twelve samples 1–4# and 11–18# were selected to be examined by DSC analysis, which underwent a thermal cycle of room temperature → 1300 °C → 200 °C at a rate of 10 K min^{-1} with the protection of argon. The other piece of the produced sample was examined by SEM/EDX to have the as-cast microstructure observed and the primary crystallization phase determined.

Thermodynamic modeling

The Gibbs energy of pure elements was taken from the SGTE unary database [18]. Solution phases like liquid, fcc_A1, bcc_A2, and hcp_A3 were described by substitutional solution model, where the ternary interaction parameters were not taken into account due to lack of experimental data. The Zr atom could substitute the Dy atom in the Al–Dy binary compounds AlDy, Al$_2$Dy$_3$, and AlDy$_2$, and vice versa in the Al–Zr binary compounds Al$_3$Zr$_2$, Al$_3$Zr$_4$, Al$_2$Zr$_3$, AlZr$_2$, and AlZr$_3$. Thus, these phases were modeled as Al$_x$(Dy, Zr)$_y$, with the Gibbs energy per formula unit expressed as

$$G_{\mathrm{Al}_x(\mathrm{Dy,Zr})_y} = y''_{\mathrm{Dy}}\,{}^0G_{\mathrm{Al:Dy}} + y''_{\mathrm{Zr}}\,{}^0G_{\mathrm{Al:Zr}} + y\mathrm{RT}(y''_{\mathrm{Dy}}\ln y''_{\mathrm{Dy}} + y''_{\mathrm{Zr}}\ln y''_{\mathrm{Zr}}) + y''_{\mathrm{Dy}}y''_{\mathrm{Zr}}\left(\sum_{j=0,1...}{}^jL_{\mathrm{Al:Dy,Zr}}(y''_{\mathrm{Dy}} - y''_{\mathrm{Zr}})^j\right),$$

(1)

where

$$G_{\mathrm{Al}_x\mathrm{Dy}_y} = x^0G_{\mathrm{Al}}^{\mathrm{fcc}} + y^0G_{\mathrm{Dy}}^{\mathrm{hcp}} + A + BT$$

(2)

$$G_{\mathrm{Al}_x\mathrm{Zr}_y} = x^0G_{\mathrm{Al}}^{\mathrm{fcc}} + y^0G_{\mathrm{Zr}}^{\mathrm{hcp}} + C + DT$$

(3)

If the phase to be modeled is an Al–Dy binary compound, $G_{\mathrm{Al}_x\mathrm{Dy}_y}$ is the Gibbs energy of Al$_x$Dy$_y$ per formula unit, and $G_{\mathrm{Al}_x\mathrm{Zr}_y}$ equals to that of a fictitious phase Al$_x$Zr$_y$ with the structure of Al$_x$Dy$_y$. In this case, the value of C which relates to enthalpy of formation of the Al$_x$Zr$_y$ phase is adopted from the first-principles calculation result and D needs to be optimized. If it is an Al–Zr binary compound, $G_{\mathrm{Al}_x\mathrm{Zr}_y}$ is the Gibbs energy of Al$_x$Zr$_y$ per formula unit, and $G_{\mathrm{Al}_x\mathrm{Dy}_y}$ equals to that of a fictitious phase Al$_x$Dy$_y$ with the structure of Al$_x$Zr$_y$. The value of A is taken from the first-principles result and B is to be optimized. The enthalpy of

formation of metastable Al–Zr and Al–Dy compounds involved in the sublattice model was calculated by the Vienna Ab-initio simulation package (VASP) [19, 20] software. The potential functions used in this calculation are Al, Dy_3, and Zr_sv. More details on the first-principles calculation have been presented in our previous work [17].

For the AlZr phase, the solubility of Dy in it was not measured in the experiments and it shows great stability during the optimization process. Even a little bit solubility of Dy could result in a three-phase equilibrium of AlZr, AlDy$_2$, and Dy at 873 K, which contradicts the phase relations that have been experimentally determined in this work. Thus, the solubility of Dy in the AlZr phase is not considered and the thermodynamic model for this phase is exactly the same as that used in the Al–Zr binary system. Likewise, without experimental evidence, the solubility of Dy in the Al$_3$Zr$_4$ phase is also not taken into account.

Results and discussion

Experimentation aspect

Figure 1 presents the backscattered electron images of annealed samples 1#, 2#, 4#, 7#, 10#, 12#, 15#, and 16#. They all consist of three equilibrium phases, which were analyzed by SEM/EDX and labeled in Fig. 1. Since the diffusion of the Dy and Zr atoms was much slower than that of the Al atom at 873 K, it is difficult to achieve a complete equilibrium state for certain samples. Therefore, some phases with a homogeneity range did not show uniform contrast. The Al$_{30}$Dy$_7$Zr$_3$ phase, ever reported in previous studies, shows two contrasts in Fig. 1a. One is light gray, which has been labeled, and the other is gray, shaped as bands in the upper left. The composition of the gray phase deviates from the stoichiometry of Al$_{30}$Dy$_7$Zr$_3$, with a nearly equi-atomic ratio of Dy and Zr. The dark gray phase with an irregular shape is caused by impurities. In Fig. 1e, the Al$_2$Dy phase also shows two contrasts. Around the dark gray Al$_2$Dy phase that has been labeled, there is the light gray one with less content of Zr. Table 2 summarizes the equilibrium phase constitution and the compositions of equilibrium phases of all the samples except 11#, 13#, and 15#. To be noted, one of the constituent phases in the samples 12# and 14#, identified as AlZr by XRD, is so slim that it is impossible for the SEM/EDX analysis to produce a reliable result on the content of constituent elements. Therefore, whether there is solubility of Dy in the AlZr phase remains unknown. Moreover, the maximum solubility of Dy in the Al$_3$Zr$_4$ phase was not known either since no sample was designed in a three-phase field with Al$_3$Zr$_4$ as an equilibrium phase. Apart
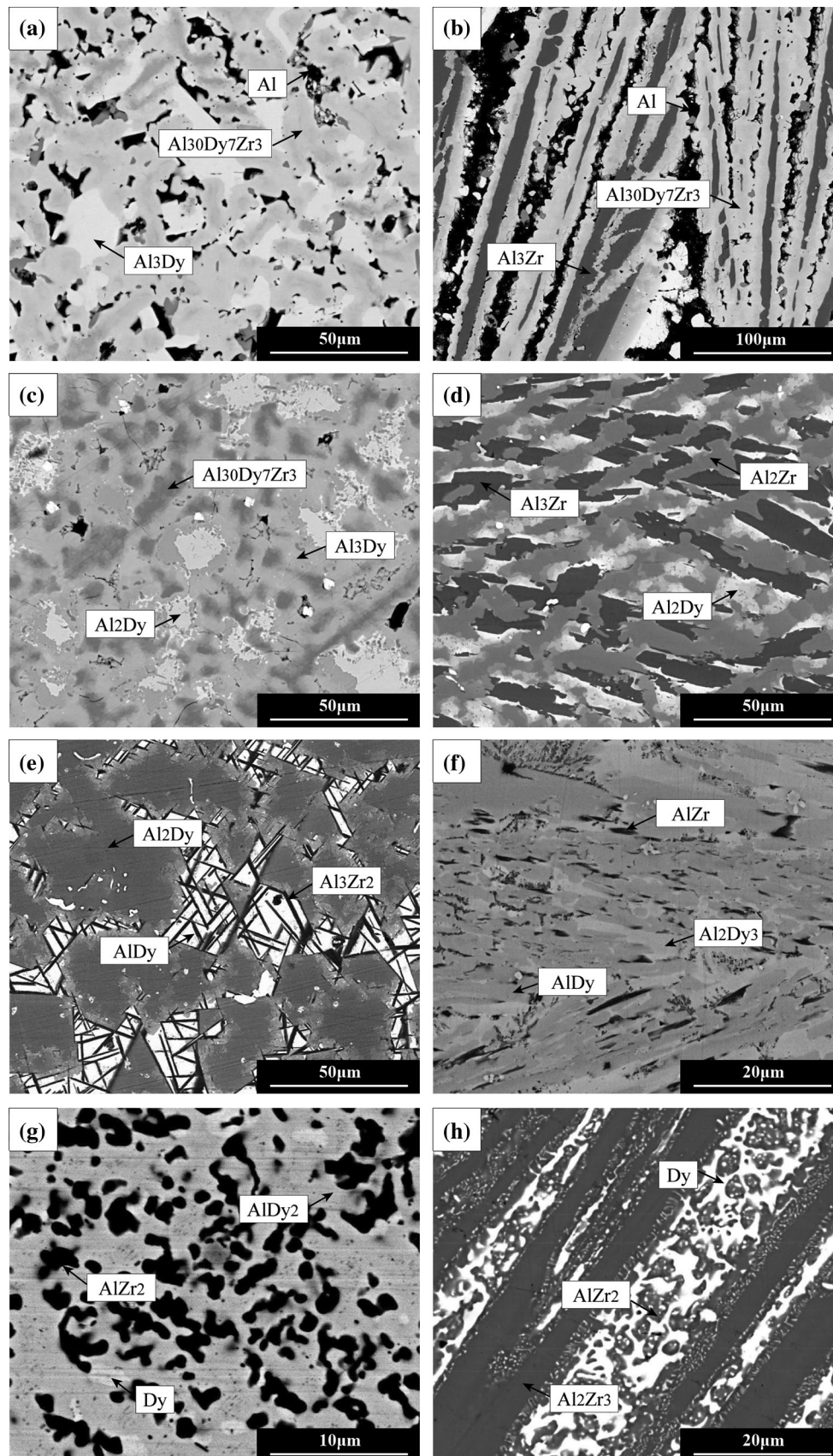
◄**Fig. 1** Backscattered electron images of the annealed samples: **a** 1#; **b** 2#; **c** 4#; **d** 7#; **e** 10#; **f** 12#; **g** 15#; **h** 16#

Table 2 Equilibrium phase constitution and compositions of constituent phases measured in this work

Alloy no.	Phase	Al (at.)	Dy (at.)	Zr (at.)
1#	fcc_Al	0.986	0.012	0.002
	Al$_3$Dy	0.762	0.223	0.015
	Al$_{30}$Dy$_7$Zr$_3$	0.760	0.178	0.062
2#	fcc_Al	0.999	0.001	0.000
	Al$_{30}$Dy$_7$Zr$_3$	0.763	0.164	0.073
	Al$_3$Zr	0.747	0.017	0.236
3#	fcc_Al	0.993	0.004	0.003
	Al$_{30}$Dy$_7$Zr$_3$	0.762	0.160	0.078
	Al$_3$Zr	0.744	0.012	0.244
4#	Al$_3$Dy	0.764	0.218	0.018
	Al$_{30}$Dy$_7$Zr$_3$	0.765	0.162	0.073
	Al$_2$Dy	0.680	0.285	0.035
5#	Al$_{30}$Dy$_7$Zr$_3$	0.763	0.160	0.077
	Al$_3$Zr	0.748	0.024	0.228
	Al$_2$Dy	0.674	0.173	0.153
6#	Al$_{30}$Dy$_7$Zr$_3$	0.757	0.163	0.080
	Al$_2$Dy	0.679	0.237	0.084
7#	Al$_3$Zr	0.743	0.014	0.243
	Al$_2$Dy	0.676	0.127	0.197
	Al$_2$Zr	0.665	0.018	0.317
8#	Al$_2$Dy	0.657	0.118	0.225
	Al$_3$Zr$_2$	0.600	0.043	0.357
9#	Al$_2$Dy	0.673	0.092	0.235
	Al$_2$Zr	0.662	0.021	0.317
	Al$_3$Zr$_2$	0.604	0.042	0.354
10#	Al$_2$Dy	0.676	0.230	0.094
	Al$_3$Zr$_2$	0.595	0.096	0.309
	AlDy	0.510	0.431	0.059
12#	AlDy	0.517	0.415	0.068
	AlZr	–	–	–
	Al$_2$Dy$_3$	0.408	0.496	0.096
14#	Al$_2$Dy$_3$	0.396	0.486	0.118
	AlZr	–	–	–
16#	Al$_2$Zr$_3$	0.397	0.024	0.579
	AlZr$_2$	0.319	0.065	0.616
	hcp_Dy	0.043	0.895	0.062
17#	AlZr$_2$	0.326	0.032	0.642
	AlZr$_3$	0.256	0.037	0.707
	hcp_Dy	0.034	0.882	0.084
18#	AlZr$_3$	0.232	0.043	0.725
	hcp_Zr	0.030	0.056	0.914
	hcp_Dy	0.023	0.885	0.092

from AlZr and Al$_3$Zr$_4$, the solubility of a third element in other Al–Dy and Al–Zr binary compounds was determined in the experiments. The corresponding XRD patterns of these samples are shown in Fig. 2. Since there are no powder diffraction files (PDFs) of the Al$_{30}$Dy$_7$Zr$_3$ and AlDy$_2$ phases, the XRD patterns were first simulated based on their crystal structure, and then used to fit the XRD patterns of the samples containing these two phases. It should be noted that the peaks of the PDF of the Al$_2$Dy phase were shifted to the right when fitting the XRD pattern of the sample 7# due to the large solubility of Zr, whereas those of the calculated PDF of the AlHo$_2$ phase were shifted to the left when analyzing the XRD pattern of the sample 15# because of the larger radius of the Dy atom than that of Ho. The equilibrium phase constitution obtained from the XRD analysis is in agreement with that from the SEM/EDX results.

It is found in this work that the phase relations determined by the samples 11# and 13# are in contradiction with those by the samples 12# and 14#. The results of SEM/EDX and XRD for the sample 11# show the existence of three phases Al$_3$Zr$_2$, AlDy, and Al$_3$Zr$_4$. For the sample 13#, the same three phases were detected by SEM/EDX, while the Al$_4$Zr$_5$ phase was discovered besides them by XRD. Through the observation of the as-cast microstructure of it, the Al$_4$Zr$_5$ phase crystallized first during solidification, indicating that the primary crystallization phase was not fully reacted. In the samples of 12# and 14#, the AlZr phase was detected, which is positioned between the Al$_3$Zr$_2$ and Al$_3$Zr$_4$ compounds in the Al–Zr binary system. Thus, the phase regions determined by the samples 12# and 14# intersect with those by the samples 11# and 13#, which violates the phase rule. As has been mentioned above, the AlZr phase was found extremely stable during the optimization process, which indicates that the phase relations determined by the samples 12# and 14# are reasonable from the thermodynamic point of view. In addition, the SEM/EDX and XRD results of the sample 15# give a consistent phase constitution, namely AlDy$_2$, Dy, and AlZr$_2$. However, this contradicts the phase relations determined by the sample 16# and thus is not considered in this work. The solubility of Zr in the AlDy$_2$ phase was measured to be about 3.4 at.%, which provides a reference for the optimization of its homogeneity range.

Modeling aspect

The optimization of the Al–Dy–Zr ternary system was carried out on the Parrot module developed by Sundman et al. [21], with the thermodynamic descriptions of Al–Dy and Dy–Zr systems taking from our previous work [17] and
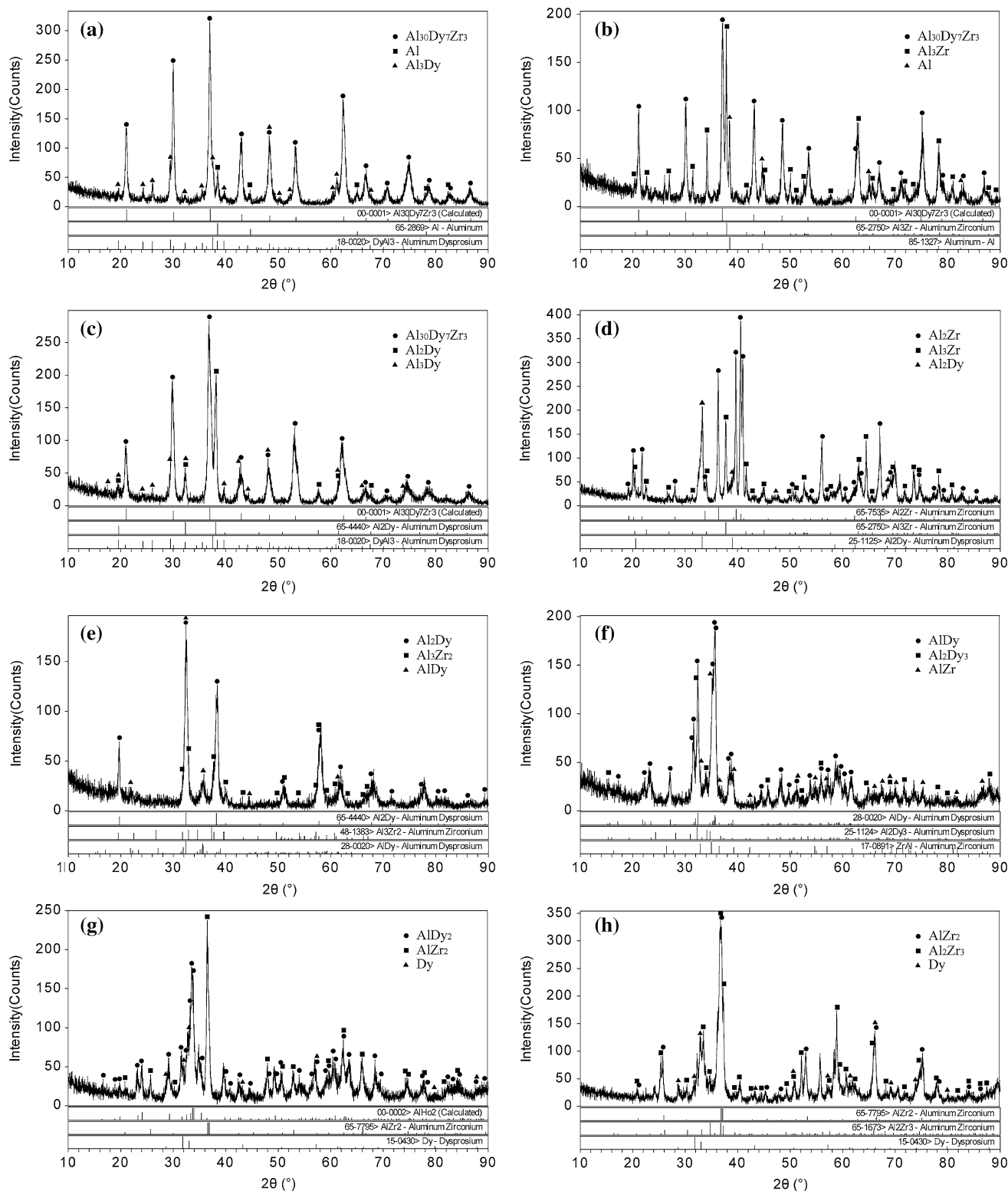
Fig. 2 XRD patterns of the annealed samples: a 1#; b 2#; c 4#; d 7#; e 10#; f 12#; g 15#; h 16#

that of the Al–Zr system from the work of Wang et al. [22]. The optimized thermodynamic parameters of the Al–Dy–Zr system are listed in Table 3.

Figure 3 presents the calculated isothermal section at 873 K, where the ternary compound $Al_{30}Dy_7Zr_3$ is designated with τ_1. The compositions of the alloys and the

Table 3 Thermodynamic parameters of the Al–Dy–Zr system optimized in this work

| Phase	Thermodynamic parameters
Al$_2$Dy: (Al, Dy, Zr)$_2$(Al, Dy, Zr)$_1$	$G_{\text{Dy:Zr}}^{\text{Al}_2\text{Dy}} = 100000 + 2 {}^0G_{\text{Dy}}^{\text{hcp}} + {}^0G_{\text{Zr}}^{\text{hcp}}$
	$G_{\text{Zr:Dy}}^{\text{Al}_2\text{Dy}} = 100000 + 2 {}^0G_{\text{Zr}}^{\text{hcp}} + {}^0G_{\text{Dy}}^{\text{hcp}}$
AlDy: (Al)$_1$(Dy, Zr)$_1$	$G_{\text{Al:Zr}}^{\text{AlDy}} = -85316 + 7.17T + {}^0G_{\text{Al}}^{\text{fcc}} + {}^0G_{\text{Zr}}^{\text{hcp}}$
	${}^0L_{\text{Al:Dy,Zr}}^{\text{AlDy}} = -22000$
Al$_2$Dy$_3$: (Al)$_2$(Dy, Zr)$_3$	$G_{\text{Al:Zr}}^{\text{Al}_2\text{Dy}_3} = -193179 + 6.10T + 2 {}^0G_{\text{Al}}^{\text{fcc}} + 3 {}^0G_{\text{Zr}}^{\text{hcp}}$
	${}^0L_{\text{Al:Dy,Zr}}^{\text{Al}_2\text{Dy}_3} = -45000$
AlDy$_2$: (Al)$_1$(Dy, Zr)$_2$	$G_{\text{Al:Zr}}^{\text{AlDy}_2} = -104576 + 6.98T + {}^0G_{\text{Al}}^{\text{fcc}} + 2 {}^0G_{\text{Zr}}^{\text{hcp}}$
	${}^0L_{\text{Al:Dy,Zr}}^{\text{AlDy}_2} = -2000$
Al$_3$Zr$_2$: (Al)$_3$(Zr, Dy)$_2$	$G_{\text{Al:Dy}}^{\text{Al}_3\text{Zr}_2} = -216155 + 150T + 3 {}^0G_{\text{Al}}^{\text{fcc}} + 2 {}^0G_{\text{Dy}}^{\text{hcp}}$
	${}^0L_{\text{Al:Zr,Dy}}^{\text{Al}_3\text{Zr}_2} = -190000$
Al$_2$Zr$_3$: (Al)$_2$(Zr, Dy)$_3$	$G_{\text{Al:Dy}}^{\text{Al}_2\text{Zr}_3} = -161207 + 25.64T + 2 {}^0G_{\text{Al}}^{\text{fcc}} + 3 {}^0G_{\text{Dy}}^{\text{hcp}}$
	${}^0L_{\text{Al:Zr,Dy}}^{\text{Al}_2\text{Zr}_3} = 33200$
AlZr$_2$: (Al)$_1$(Zr, Dy)$_2$	$G_{\text{Al:Dy}}^{\text{AlZr}_2} = -80412 + 16.77T + {}^0G_{\text{Al}}^{\text{fcc}} + 2 {}^0G_{\text{Dy}}^{\text{hcp}}$
	${}^0L_{\text{Al:Zr,Dy}}^{\text{AlZr}_2} = -3000$
AlZr$_3$: (Al)$_1$(Zr, Dy)$_3$	$G_{\text{Al:Dy}}^{\text{AlZr}_3} = -78688 + 20T + {}^0G_{\text{Al}}^{\text{fcc}} + 3 {}^0G_{\text{Dy}}^{\text{hcp}}$
	${}^0L_{\text{Al:Zr,Dy}}^{\text{AlZr}_3} = -4000$
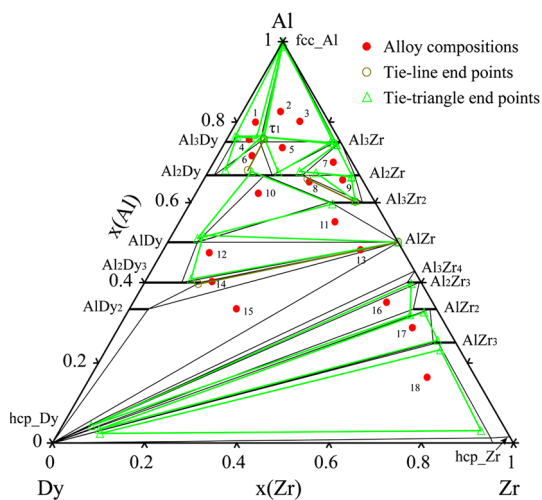
Fig. 3 Calculated isothermal section of the Al–Dy–Zr system at 873 K superimposed with the experimental data of this work

Fig. 4 Calculated isothermal section of the Al–Dy–Zr system at 773 K

constituent equilibrium phases in each sample are superimposed in the figure. For the AlZr phase whose composition was not determined by SEM/EDX, the end points of the tie-line and tie-triangle with regard to it are plotted at $x_{\text{Al}} = 0.5$ and $x_{\text{Zr}} = 0.5$. The calculated phase relations agree very well with the experimental results. Figure 4 shows the calculated isothermal section of the Al–Dy–Zr system at 773 K, which is superimposed with the experimental data of Yuan et al. [14] and Hu et al. [15]. The calculated phase relations in the Al–Al$_2$Dy–Al$_2$Zr and Dy–
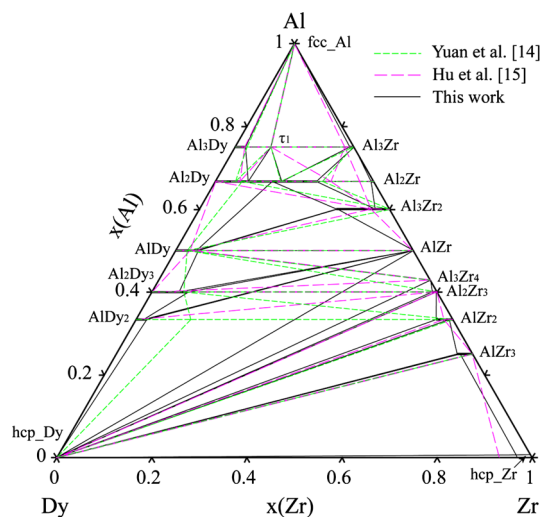
Zr–AlZr$_2$ regions are consistent with their experimental results, and the three-phase equilibrium of Dy, Al$_2$Zr$_3$, and AlZr$_2$ reported by Hu et al. [15] is confirmed. For the rest regions, the measured phase relations could not be reproduced with any thermodynamic parameters, which means that they are not valid from the perspective of thermodynamics. In addition, there is a disagreement in the homogeneity range of Al–Dy and Al–Zr binary compounds among the calculation results of this work and the experimental results of Yuan et al. [14] and Hu et al. [15]. In the

present work, all of the binary compounds show a solubility of the third component except AlZr and Al_3Zr_4, which is not the case in the other work according to the review in "Review of the Al–Dy–Zr ternary system" section. The reason for the difference in the phase relations of the Dy–AlDy–AlZr–AlZr$_2$–Dy region among the three studies may be attributed to the thermal history that samples have been subjected to before the quench. According to Yuan et al. [14], the samples were annealed at 873 K for 15 h, followed by a 720 h annealing at 773 K. In the work of Hu et al. [15], the annealing for most samples was first carried out at 1073 K for 720 h, and then at 773 K for 350 h, and samples with more than 75 at.% Al were annealed at 900 K for 960 h, and then at 773 K for 350 h. They both employed a two-order homogenization treatment, a homogenization at a high temperature followed by one at the low temperature of interest to reach the final equilibrium. One thing that should be concerned is the influence of the high-temperature annealing on the microstructure finally obtained. How long it takes for the final annealing to eliminate this impact is unknown for this kind of treatment. In the present work, the samples were all annealed at 873 K for 1440 h. Since they were annealed at a higher temperature than the final annealing temperature of other work for a longer time, a state that is closer to the equilibrium should be expected at the temperature under study. Thus, during the optimization, the experimental results of our work were mainly considered. On this basis, the experimental data of Yuan et al. [14] and Hu et al. [15] that do not contradict those of the present work were reproduced. The DSC curves of heating and cooling were all analyzed. The phase transition temperatures were determined from the onset of the thermal arrest during heating and the end of it during cooling. Vertical sections that contain each sample were calculated respectively and the DSC data were superimposed to make a better interpretation of the DSC signals. Figure 5 presents the vertical section at 80 at.% Al of the Al–Dy–Zr system and a comparison was made between the calculation result and the DSC data for the samples 1# and 3#. The calculated vertical section at 9 at.% Dy is shown in Fig. 6, where the DSC data for the samples 13# and 2# are given as well. The calculated phase transformation temperatures of the four alloys above are generally in good agreement with the DSC results.

With the optimized thermodynamic parameters for the Al–Dy–Zr system, the liquidus projection was calculated, as shown in Fig. 7. The calculated primary crystallization phases are labeled in the figure and the observed ones in the as-cast samples in the legend. Good fit is found between the calculation results and the experimental observations for all the samples except 11#, 12#, and 17#. The primary crystallization phases for the samples 11# and 17# were
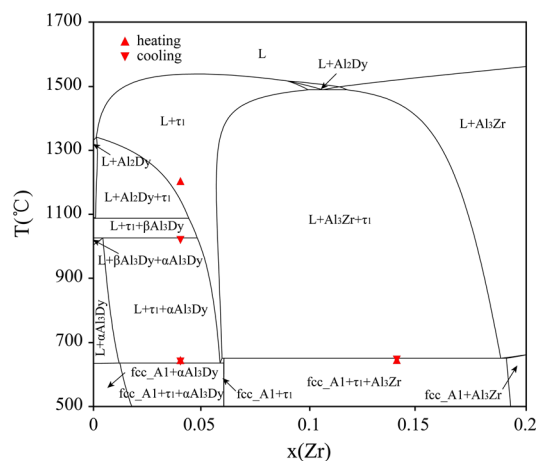

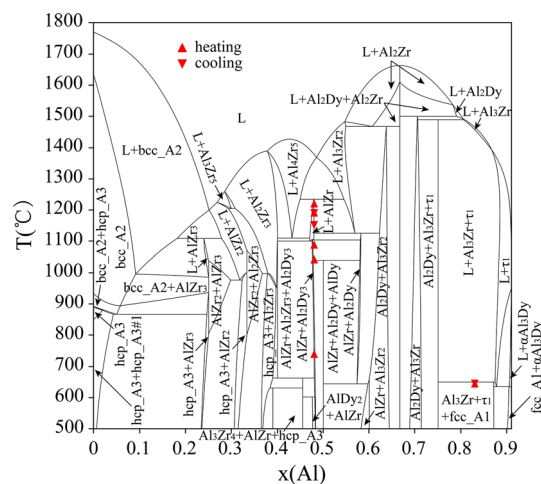**Fig. 5** Calculated vertical section of the Al–Dy–Zr system at 80 at.% Al

Fig. 6 Calculated vertical section of the Al–Dy–Zr system at 9 at.% Dy

calculated to be Al_2Dy and Al_3Zr_5, respectively, while they were found to be Al_3Zr_2 and $AlZr_2$ in the experiments. As can be seen from Fig. 7, the primary crystallization fields of Al_2Dy and Al_3Zr_2 are adjacent with each other, and it is the same case with those of Al_3Zr_5 and $AlZr_2$. The position of the samples in the composition triangle is so close to the boundary of the observed primary crystallization fields that it is reasonable to accept the calculation results. For the sample 12#, the calculated and observed primary crystallization phases are Al_2Dy and $AlDy$, respectively, and the deviation between the calculated and experimental results is a little larger than that for the samples 11# and 17#. Attempts have been made in vain to reduce the primary crystallization field of the Al_2Dy phase, which would be accompanied by a decrease in the solubility of Zr in the Al_2Dy phase at 873 K, leading to a poor fit with the experimental data. Three enlarged portions are also shown
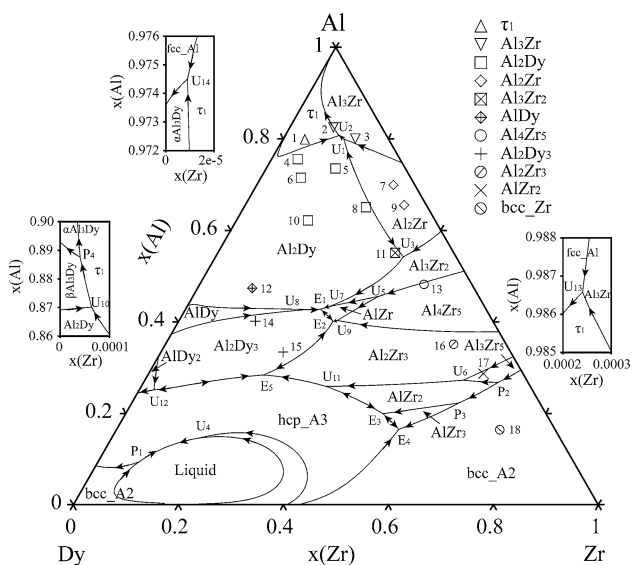
Fig. 7 Calculated liquidus projection of the Al–Dy–Zr system together with the primary crystallization phases observed in the as-cast samples

in Fig. 7 in order to present the ternary invariant reactions in the Al-rich corner clearly. The calculated invariant reactions and their temperatures of the Al–Dy–Zr ternary

system are listed in Table 4. For comparison, the experimental phase transition temperatures are given as well, which are determined from the onset of the thermal arrest during heating unless otherwise specified. The differences between the calculated and measured temperatures of invariant reactions are all within 14 °C, except the reaction P_3, for which the difference is 21 °C.

Conclusions

The isothermal section of the Al–Dy–Zr system at 873 K has been established using individual alloys. The ternary compound $Al_{30}Dy_7Zr_3$ with an $L1_2$ structure reported in previous studies still exists at this temperature. Solubility of a third element was found in all the Al–Dy and Al–Zr binary compounds with an exception of AlZr and Al_3Zr_4, where the solubility of Dy was not determined in this work. Besides the isothermal section, DSC analysis was conducted to extract phase transformation temperatures. The microstructure of the as-cast samples was also observed to identify the primary crystallization phases. Based on the experimental information above and the first-principles calculation results on the enthalpy of formation of the

Table 4 Calculated invariant reactions of the Al–Dy–Zr system

Type	Reaction	T (°C) (Cal./Exp.)
U_1	Liquid + Al_2Zr ↔ Al_2Dy + Al_3Zr	1499
U_2	Liquid + Al_2Dy ↔ τ_1 + Al_3Zr	1488
U_3	Liquid + Al_2Zr ↔ Al_2Dy + Al_3Zr_2	1467
U_4	Liquid + bcc_A2 ↔ Liquid #1 + hcp_A3	1308
P_1	Liquid + Liquid #1 + bcc_A2 ↔ hcp_A3	1308
P_2	Liquid + bcc_A2 + Al_3Zr_5 ↔ $AlZr_2$	1242
U_5	Al_3Zr_2 + Al_4Zr_5 ↔ Liquid + AlZr	1233/1220
U_6	Liquid + Al_3Zr_5 ↔ $AlZr_2$ + Al_2Zr_3	1204
U_7	Liquid + Al_3Zr_2 ↔ Al_2Dy + AlZr	1125
U_8	Liquid + AlDy ↔ Al_2Dy_3 + Al_2Dy	1111
U_9	Liquid + Al_4Zr_5 ↔ AlZr + Al_2Zr_3	1109
P_3	Liquid + $AlZr_2$ + bcc_A2 ↔ $AlZr_3$	1108/1129[a]
E_1	Liquid ↔ AlZr + Al_2Dy_3 + Al_2Dy	1103/1089
E_2	Liquid ↔ AlZr + Al_2Zr_3 + Al_2Dy_3	1100
U_{10}	Liquid + Al_2Dy ↔ τ_1 + βAl_3Dy	1087
P_4	Liquid + τ_1 + βAl_3Dy ↔ αAl_3Dy	1025/1019
U_{11}	Liquid + $AlZr_2$ ↔ Al_2Zr_3 + hcp_A3	997
E_3	Liquid ↔ hcp_A3 + $AlZr_2$ + $AlZr_3$	976
E_4	Liquid ↔ $AlZr_3$ + bcc_A2 + hcp_A3	963/950
E_5	Liquid ↔ Al_2Zr_3 + Al_2Dy_3 + hcp_A3	952/966
U_{12}	Liquid + Al_2Dy_3 ↔ hcp_A3 + $AlDy_2$	945
U_{13}	Liquid + Al_3Zr ↔ τ_1 + fcc_A1	649/645
U_{14}	Liquid + τ_1 ↔ fcc_A1 + αAl_3Dy	634/644

[a] The measured phase transition temperature was determined from the DSC curve during cooling

metastable end-member in the sublattice model, the phase diagram of the Al–Dy–Zr ternary system was optimized with the CALPHAD method. Not only are the calculated isothermal section at 873 K and the vertical sections at 80 at.% Al and 9 at.% Dy in good agreement with the experimental results, but also most of the observed primary crystallization phases could be well accounted for by the calculated liquidus projection. It should be mentioned that the three-phase equilibria of $AlZr + Al_2Dy_3 + AlDy_2$ and $AlZr + AlDy_2 + Al_2Zr_3$ at 873 K are lack in experimental evidence and further experimental investigation is needed. The phase relations in the $Dy–AlDy–AlZr–Al_2Zr_3$–Dy region at 773 K reported in literatures could not be reproduced with any thermodynamic parameters, indicating that they should not exist from the thermodynamic point of view.

References

1. Gao T, Zhang YR, Liu XF (2014) Influence of trace Ti on the microstructure, age hardening behavior and mechanical properties of an Al-Zn-Mg-Cu-Zr alloy. Mater Sci Eng A 598:293–298

2. Fang HC, Chen KH, Chen X, Huang LP, Peng GS, Huang BY (2011) Effect of Zr, Cr and Pr additions on microstructures and properties of ultra-high strength Al-Zn-Mg-Cu alloys. Mater Sci Eng A 528:7606–7615

3. Jiang L, Li JK, Cheng PM, Liu G, Wang RH, Chen BA, Zhang JY, Sun J, Yang MX, Yang G (2014) Microalloying ultrafine grained Al alloys with enhanced ductility. Sci Rep 4:3605-1–3605-6

4. Chen KH, Fang HC, Zhang Z, Chen X, Liu G (2008) Effect of Yb, Cr and Zr additions on recrystallization and corrosion resistance of Al-Zn-Mg-Cu alloys. Mater Sci Eng A 497:426–431

5. Woo KD, Kim SW (2002) The mechanical properties and precipitation behavior of an Al-Cu-Li-(In, Be) alloy. J Mater Sci 37:411–416. doi:10.1023/A:1013633219939

6. Liao ZQ, Li SC, Zheng ZQ, Cai B, Zhong S, Luo XF (2012) The effect of Ge addition on Al-3.5Cu-0.4 Mg (wt.%) alloy. Scr Mater 66:447–450

7. Vo NQ, Dunand DC, Seidman DN (2014) Improving aging and creep resistance in a dilute Al-Sc alloy by microalloying with Si, Zr and Er. Acta Mater 63:73–85

8. Booth-Morrison C, Mao Z, Diaz M, Dunand DC, Wolverton C, Seidman DN (2012) Role of silicon in accelerating the nucleation of Al₃(Sc, Zr) precipitates in dilute Al-Sc-Zr alloys. Acta Mater 60:4740–4752

9. Krug ME, Werber A, Dunand DC, Seidman DN (2010) Core-shell nanoscale precipitates in Al-0.06 at.% Sc microalloyed with Tb, Ho, Tm or Lu. Acta Mater 58:134–145

10. Karnesky RA, van Dalen ME, Dunand DC, Seidman DN (2006) Effects of substituting rare-earth elements for scandium in a precipitation-strengthened Al-0.08 at.% Sc alloy. Scr Mater 55:437–440

11. van Dalen ME, Dunand DC, Seidman DN (2006) Nanoscale precipitation and mechanical properties of Al-0.06 % Sc alloys microalloyed with Yb or Gd. J Mater Sci 41:7814–7823. doi:10.1007/s10853-006-0664-9

12. Knipling KE, Dunand DC, Seidman DN (2006) Criteria for developing castable, creep-resistant aluminum-based alloys-a review. Z Metallkd 97:246–265

13. Tyvanchuk AT, Procik AS (1982) Ternary phase diagrams Al-(Tb, Dy, Ho)-(Zr, Hf) for the concentration range 67–100 at.% Al. Dopov Akad Nauk Ukrain RSR Ser B 11:62–64

14. Yuan XL, Liu LB, Cai GM, Bo H, Cao FY, Zheng F (2011) Isothermal section of the Al-Dy-Zr ternary system at 773 K. J Alloys Compd 509:6190–6195

15. Hu ZH, Zhan YZ, Ling MX, Liang Y, Liu Y, Wei SJ, Du Y (2012) Phase diagram of the Al-Dy-Zr ternary system at 773 K. Int J Mat Res 103:853–857

16. Pang MJ, Zhan YZ, Yang WC, Li CL, Du Y (2010) The phase relationships in the Al-Zr-Ho ternary system at 773 K. J Alloys Compd 508:79–84

17. Bo H, Liu LB, Xiong X, Jin ZP (2014) Thermodynamic assessment of the Al-Dy, Dy-Zr and Al-Dy-Zr systems. Chin Sci Bull 59:1738–1746

18. Dinsdale AT (2001) SGTE unary database, version 4.4

19. Kresse G, Furthmüller J (1996) Efficient iterative schemes for ab initio total-energy calculations using a plane-wave basis set. Phys Rev B 54:11169–11186

20. Kresse G, Furthmüller J (1996) Efficiency of ab initio total energy calculations for metals and semi-conductors using a plane-wave basis set. Comput Mater Sci 6:15–50

21. Sundman B, Jansson B, Andersson JO (1985) The thermo-calc databank system. CALPHAD 9:153–190

22. Wang T, Jin ZP, Zhao JC (2001) Thermodynamic assessment of the Al-Zr binary system. J Phase Equilib 22:544–551